Inorganic Chemistry

Article

pubs.acs.org/IC

Synthesis, Structures, and Optical Properties of Ruthenium(II) Complexes of the Tris(1-pyrazolyl)methane Ligand

Benjamin J. Coe,*[,†] Madeleine Helliwell,[†] Martyn K. Peers,[†] James Raftery,[†] Daniela Rusanova,[†] Koen Clays,[‡] Griet Depotter,[‡] and Bruce S. Brunschwig[§]

[†]School of Chemistry, University of Manchester, Oxford Road, Manchester M13 9PL, U.K.

[‡]Department of Chemistry, University of Leuven, Celestijnenlaan 200D, B-3001 Leuven, Flanders, Belgium

[§]Molecular Materials Research Center, Beckman Institute, MC 139-74, California Institute of Technology, 1200 East California Boulevard, Pasadena, California 91125, United States

Supporting Information

ABSTRACT: Four new complex salts $[Ru^{II}Cl(Tpm)(L^A)_2][PF_6]_n$ [Tpm = tris(1-pyrazolyl)methane; n = 1, L^A = pyridine (py) **1** or ethyl isonicotinate (EIN) **2**; n = 3, L^A = *N*-methyl-4,4′-bipyridinium (MeQ^+) **3** or *N*-phenyl-4,4′-bipyridinium (PhQ^+) **4**] have been prepared and characterized. Electronic absorption spectra show intense d → π^* metal-to-ligand charge-transfer (MLCT) absorption bands, while cyclic voltammetry reveals a reversible $Ru^{III/II}$ wave, accompanied by quasireversible or irreversible L^A-based reductions for all except **1**. Single crystal X-ray structures have been obtained for **1**•Me_2CO, **2**, and **3**•Me_2CO. For **2**−**4**, molecular first hyperpolarizabilities β have been measured in acetonitrile solutions via the hyper-Rayleigh scattering (HRS) technique at 800 nm. Stark (electroabsorption) spectroscopic studies on the MLCT bands in frozen butyronitrile allow the indirect estimation of static first hyperpolarizabilities β_0. The various physical data obtained for **3** and **4** are compared with those reported previously for related *cis*-$\{Ru^{II}(NH_3)_4\}^{2+}$ species [Coe, B. J. et al. *J. Am. Chem. Soc.* **2005**, *127*, 4845]. TD-DFT calculations on the complexes in **1**−**4** confirm that their lowest energy absorption bands are primarily Ru^{II} → L^A MLCT in character, while Ru^{II} → Tpm MLCT transitions are predicted at higher energies. DFT agrees with the Stark, but not the HRS measurements, in showing that β_0 increases with the electron-accepting strength of L^A. The 2D nature of the chromophores is evidenced by dominant β_{xxy} tensor components.

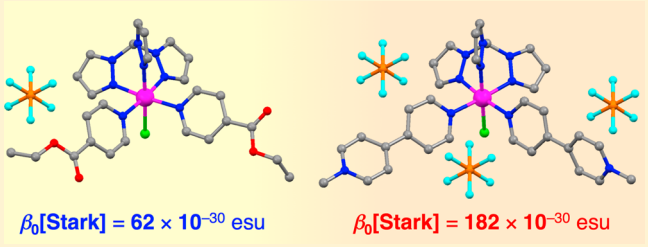

INTRODUCTION

The precious metal ruthenium exhibits a particularly rich coordination and organometallic chemistry, encompassing a huge range of stable complexes with every type of ligand imaginable.[1] The relatively high stability and comparative ease of synthesis of Ru complexes has allowed this area of chemistry to develop freely. Besides their fundamental scientific value, such complexes are of interest for practical applications in various important fields including catalysis,[2] biology/medicine,[3] and technologies that rely upon the photophysical/chemical properties of Ru^{II}-containing chromophores.[4] The latter cover themes such as organic light-emitting diodes[5] and dye-sensitized solar cells,[6] which typically involve complexes of chelating polypyridyl ligands, especially 2,2′-bipyridyl. Such species have fascinating electronic absorption, emission, and electron/energy-transfer properties that are based on low energy metal-to-ligand charge-transfer (MLCT) excited states. Tuning the properties of these states by judicious changes in ligand structure has become a highly developed area of coordination chemistry.[4]

In addition to the above-mentioned areas, Ru complexes have attracted attention for their nonlinear optical (NLO) behavior.[7] Such phenomena involve changing the fundamental properties of laser beams, useful in harmonic generators and electrooptic switches, with emerging applications like biological imaging.[8] Our ongoing investigations in this field have included a series of complexes with V-shaped dipolar structures based on electron-donating *cis*-$\{Ru^{II}(NH_3)_4\}^{2+}$ centers.[9] These complexes show intense, broad MLCT absorption profiles in the visible region, comprising overlapping bands. The MLCT transitions are associated with relatively large quadratic (second-order) NLO responses. Ru^{II} complexes of the tris(1-pyrazolyl)methane (Tpm) ligand have been studied quite extensively,[10] and using such a ligand which most commonly coordinates in a tridentate, facial manner offers possibilities for binding various other ligands in a mutually cis orientation. The present study involves a series of new $Ru^{II}Cl(Tpm)$ complexes with two pyridine or pyridyl coligands. The optical spectroscopic, electrochemical, and NLO properties of two of these new species are compared

Received: January 21, 2014
Published: March 10, 2014

   dx.doi.org/10.1021/ic500145r | *Inorg. Chem.* 2014, 53, 3798−3811

with those of their *cis*-$\{Ru^{II}(NH_3)_4\}^{2+}$ analogues, and several X-ray crystallographic studies are presented.

EXPERIMENTAL SECTION

Materials and Procedures. The compounds Tpm,[11] $Ru^{II}Cl_3(Tpm)\bullet 1.5H_2O$,[12] $[Ru^{II}Cl_2(Tpm)(NO)]PF_6$,[13] *N*-methyl-4,4′-bipyridinium hexafluorophosphate ($[MeQ^+]PF_6$),[14] and *N*-phenyl-4,4′-bipyridinium chloride ($[PhQ^+]Cl\bullet 2H_2O$)[15] were synthesized by following previously published methods. Tpm was recrystallized from boiling water to give white needle-like crystals in yields of ca. 70%. All other reagents were obtained commercially and used as supplied. Products were dried overnight in a vacuum desiccator (silica gel) prior to any characterization and were heated under vacuum at ca. 100 °C before CHN analyses.

General Physical Measurements. ^{1}H NMR spectra were recorded on Bruker AV-400 or DPX-300 spectrometers, with all shifts referenced to residual solvent signals and quoted with respect to TMS. The AA′BB′ patterns of pyridyl or phenyl rings are reported as simple doublets, with '*J* values' referring to the two most intense peaks. Elemental analyses were performed by the Microanalytical Laboratory, University of Manchester, and UV−vis spectra were obtained by using a Shimadzu UV-2401 PC spectrophotometer. IR spectroscopy was performed on solid samples by using an Excalibur BioRad FT-IR spectrometer, and mass spectra were recorded by using +electrospray on a Micromass Platform II spectrometer. Cyclic voltammetric measurements were performed by using an Ivium CompactStat. A single-compartment cell was used with a silver/silver chloride reference electrode (3 M NaCl, saturated AgCl) separated by a salt bridge from a glassy-carbon 2 mm disk working electrode and Pt wire auxiliary electrode. Acetonitrile was used as supplied from Sigma-Aldrich (HPLC grade), and $[N(C_4H_9\text{-}n)_4]PF_6$ (Fluka, electrochemical grade) was used as the supporting electrolyte. Solutions containing ca. 10^{-3} M analyte (0.1 M $[N(C_4H_9\text{-}n)_4]PF_6$) were deaerated by purging with N_2. All $E_{1/2}$ values were calculated from $(E_{pa} + E_{pc})/2$ at a scan rate of 100 mV s^{-1}.

Synthesis of $[Ru^{II}Cl(Tpm)(py)_2]PF_6$ (1). $[Ru^{II}Cl_2(Tpm)(NO)]PF_6$ (113 mg, 0.201 mmol), NaN_3 (13.4 mg, 0.206 mmol), pyridine (0.8 mL), and methanol (8 mL) were stirred under Ar for 1.5 h. During this time, the brown suspension became lighter in color. The mixture was then heated at reflux for 1 h, to give a clear dark yellow solution. After cooling to room temperature, a few crystals of NH_4PF_6 were added, and volatiles were removed under vacuum. The resulting brown oil was dissolved in acetone and filtered through a mixture of $MgSO_4$ and Celite, removing the NaCl byproduct. The acetone was removed under vacuum, then the sticky brown solid was dissolved in dry dichloromethane, and diethyl ether was added slowly to give a precipitate; this was filtered off, washed with diethyl ether, and dried to give a yellow solid: 100 mg, 73%; δ_H ($(CD_3)_2CO$, 400 MHz) 9.79 (1 H, s, CH), 8.78−8.76 (5 H, $C_3H_3N_2$ + $pyH^{2,6}$), 8.60 (2 H, d, J = 2.8 Hz, $C_3H_3N_2$), 8.01 (1 H, d, J = 2.3 Hz, $C_3H_3N_2$), 7.93 (2 H, t, J = 7.6 Hz, pyH^4), 7.76 (2 H, d, J = 2.2 Hz, $C_3H_3N_2$), 7.44 (4 H, t, J = 7.1 Hz, $pyH^{3,5}$), 6.77 (1 H, t, J = 2.6 Hz, $C_3H_3N_2$−H^4), 6.61 (2 H, t, J = 2.6 Hz, $C_3H_3N_2$−H^4). Anal. Calcd (%) for $C_{20}H_{20}ClF_6N_8PRu\bullet 1.5H_2O$: C, 35.3; H, 3.4; N, 16.5. Found: C, 35.4; H, 3.0; N, 16.1. m/z = 509 $[(M - PF_6)^+]$. Single crystals suitable for X-ray diffraction studies were grown by slow diffusion of diethyl ether vapor into an acetone solution at room temperature.

Synthesis of $[Ru^{II}Cl(Tpm)(EIN)_2]PF_6$ (2). $[Ru^{II}Cl_2(Tpm)(NO)]PF_6$ (111 mg, 0.198 mmol), NaN_3 (12.7 mg, 0.195 mmol), ethyl isonicotinate (EIN, 1.0 mL), and methanol (12 mL) were stirred under Ar for 1 h. During this time, the brown suspension became lighter in color and acquired an orange tint. The mixture was then heated at reflux for 1 h, to give a clear, intensely orange solution. After cooling to room temperature, the volatiles were removed under vacuum. The resulting orange oil was dissolved in acetone (5 mL), and a few crystals of NH_4PF_6 were added. The NaCl byproduct was removed by filtration through Celite, adding further acetone (10 mL). The orange solution was concentrated to 2 mL, and diethyl ether (20 mL) was added. The turbid mixture was stored in a refrigerator overnight, and then the orange precipitate was filtered off, washed with diethyl ether, and dried: 100 mg, 64%; δ_H ($(CD_3)_2CO$, 300 MHz) 9.91 (1 H, s, CH), 8.99 (4 H, d, J = 6.8 Hz, C_5H_4N), 8.80 (1 H, d, J = 3.0 Hz, $C_3H_3N_2$), 8.64 (2 H, d, J = 2.8 Hz, $C_3H_3N_2$), 8.03 (1 H, d, J = 2.3 Hz, $C_3H_3N_2$), 7.85 (4 H, d, J = 6.8 Hz, C_5H_4N), 7.80 (2 H, d, J = 2.2 Hz, $C_3H_3N_2$), 6.80 (1 H, t, J = 2.6 Hz, $C_3H_3N_2$−H^4), 6.64 (2 H, t, J = 2.6 Hz, $C_3H_3N_2$−H^4), 4.42 (4 H, q, J = 7.1 Hz, CH_2), 1.37 (6 H, t, J = 7.1 Hz, Me). ν(C═O) 1716s cm^{-1}, ν(C−O) 1277 cm^{-1}. Anal. Calcd (%) for $C_{26}H_{28}ClF_6N_8O_4PRu$: C, 39.1; H, 3.5; N, 14.0. Found: C, 38.8; H, 3.1; N, 14.0. m/z = 653 $[(M - PF_6)^+]$. Single crystals suitable for X-ray diffraction studies were grown by slow diffusion of diethyl ether vapor into a methanol solution at room temperature.

Synthesis of $[Ru^{II}Cl(Tpm)(MeQ^+)_2][PF_6]_3$ (3). $[Ru^{II}Cl_2(Tpm)(NO)]PF_6$ (110 mg, 0.196 mmol), NaN_3 (12.9 mg, 0.198 mmol), $[MeQ^+]PF_6$ (130 mg, 0.411 mmol), and methanol (15 mL) were stirred under Ar for 1 h. During this time, the brown suspension became lighter in color, changing to light purple, then dark purple. The mixture was heated at reflux for 1 h, with no further color change. The solvent was removed under vacuum, the purple residue was dissolved in acetone (10 mL), and solid NH_4PF_6 (ca. 0.1 g) was added. The purple solution was concentrated to 2 mL, and diethyl ether (25 mL) was added. The turbid mixture was stored in a refrigerator for 1.5 h, and then the dark purple precipitate was filtered off. This material was dissolved in acetone (20 mL), and the solution was filtered through Celite. The filtrate was concentrated to 2 mL, and the crude product was precipitated with diethyl ether, filtered off, washed with diethyl ether and dried. Purification was effected by using a basic alumina column, eluting with 0.05 M NH_4PF_6 in acetonitrile. The second, purple fraction was collected, evaporated to dryness, and then reprecipitated from acetone/diethyl ether to yield a dark purple solid: 98 mg, 44%; δ_H ($(CD_3)_2CO$, 400 MHz) 9.89 (1 H, s, CH), 9.23 (4 H, d, J = 6.9 Hz, C_5H_4N), 9.08 (4 H, d, J = 7.0 Hz, C_5H_4N), 8.80 (1 H, d, J = 2.5 Hz, $C_3H_3N_2$), 8.67 (4 H, d, J = 7.0 Hz, C_5H_4N), 8.65 (2 H, d, J = 3.0 Hz, $C_3H_3N_2$), 8.06 (1 H, d, J = 2.3 Hz, $C_3H_3N_2$), 8.03 (4 H, d, J = 7.0 Hz, C_5H_4N), 7.82 (2 H, d, J = 2.2 Hz, $C_3H_3N_2$), 6.81 (1 H, t, J = 2.6 Hz, $C_3H_3N_2$−H^4), 6.66 (2 H, t, J = 2.6 Hz, $C_3H_3N_2$−H^4), 4.65 (6 H, s, Me). Anal. Calcd (%) for $C_{32}H_{32}ClF_{18}N_{10}P_3Ru$: C, 34.1; H, 2.9; N, 12.4. Found: C, 33.7; H, 2.9; N, 12.2. m/z = 983 $[(M - PF_6)^+]$, 419 $[(M - 2PF_6)^{2+}]$. Single crystals suitable for X-ray diffraction studies were grown by slow diffusion of diethyl ether vapor into an acetone solution at room temperature.

Synthesis of $[Ru^{II}Cl(Tpm)(PhQ^+)_2][PF_6]_3$ (4). $Ru^{II}Cl_3(Tpm)\bullet 1.5H_2O$ (82 mg, 0.183 mmol) and $[PhQ^+]Cl\bullet 2H_2O$ (307 mg, 1.01 mmol) in 1:1 ethanol/water (degassed, 40 mL) were heated at reflux under Ar for 14 h. The initial brown suspension became blue-purple as the temperature increased. After cooling to room temperature, the volume was reduced under vacuum to ca. 10 mL, and saturated aqueous NH_4PF_6 (5 mL) was added. A dark purple, sticky precipitate formed immediately. Acetone was added, and the solution was filtered through Celite/$MgSO_4$, removing insoluble white material. The filtrate was concentrated to 3−4 mL, diethyl ether was added, and the dark purple solid was filtered off and dried. Purification was effected as for **3** to yield a dark purple solid: 97 mg, 41%; δ_H ($(CD_3)_2CO$, 400 MHz) 9.86 (1 H, s, CH), 9.53 (4 H, d, J = 7.0 Hz, C_5H_4N), 9.15 (4 H, d, J = 7.0 Hz, C_5H_4N), 8.85 (4 H, d, J = 7.0 Hz, C_5H_4N), 8.81 (1 H, d, J = 2.9 Hz, $C_3H_3N_2$), 8.66 (2 H, d, J = 2.8 Hz, $C_3H_3N_2$), 8.13 (4 H, d, J = 7.0 Hz, C_5H_4N), 8.09 (1 H, d, J = 2.2 Hz, $C_3H_3N_2$), 8.01−7.98 (4 H, Ph), 7.84−7.81 (8 H, $C_3H_3N_2$ + Ph), 6.83 (1 H, t, J = 2.6 Hz, $C_3H_3N_2$−H^4), 6.68 (2 H, t, J = 2.6 Hz, $C_3H_3N_2$−H^4). Anal. Calcd (%) for $C_{42}H_{36}ClF_{18}N_{10}P_3Ru\bullet 3H_2O$: C, 38.6; H, 3.2; N, 10.7. Found: C, 38.1; H, 2.4; N, 10.6. m/z = 1107 $[(M - PF_6)^+]$, 480 $[(M - 2PF_6)^{2+}]$.

X-ray Structural Determinations. The data were collected on a Bruker APEX CCD X-ray diffractometer by using graphite-monochromated, Mo$K\alpha$ radiation (wavelength = 0.71073 Å). Data processing was carried out by using the Bruker SAINT[16] software

dx.doi.org/10.1021/ic500145r | *Inorg. Chem.* 2014, 53, 3798−3811

Table 1. Crystallographic Data and Refinement Details for Salts 1•Me_2CO, 2, and 3•Me_2CO

	1•Me_2CO	2	3•Me_2CO
empirical formula	$C_{23}H_{26}ClF_6N_8OPRu$	$C_{26}H_{28}ClF_6N_8O_4PRu$	$C_{35}H_{38}ClF_{18}N_{10}OP_3Ru$
fw	712.01	798.05	1186.18
cryst system	monoclinic	monoclinic	monoclinic
space group	$P2_1/n$	$P2_1/n$	$P2_1/c$
space group number	14	14	14
a/Å	11.491(2)	16.2895(14)	22.7148(19)
b/Å	8.5395(17)	7.7203(7)	11.6324(10)
c/Å	28.167(6)	26.279(2)	17.5531(15)
α/deg			
β/deg	97.888(4)	104.064(2)	108.045(2)
γ/deg			
U/Å^3	2737.7(9)	3205.8(5)	4409.9(6)
Z	4	4	4
T/K	100(2)	100(2)	100(2)
μ/mm^{-1}	0.805	0.704	0.647
cryst size/mm	0.20 × 0.10 × 0.05	0.18 × 0.08 × 0.02	0.20 × 0.12 × 0.08
cryst description	yellow plate	amber plate	purple block
reflns collected	19005	22347	37416
independent reflns (R_{int})	4828 (0.1035)	5672 (0.0940)	10350 (0.0915)
θ_{max}/deg (completeness)	25.03 (99.9)	25.00 (99.9)	25.00 (99.8)
reflns with $I > 2\sigma(I)$	3023	4319	5534
GOF on F^2	0.923	1.282	0.885
final $R1$, $wR2$ [$I > 2\sigma(I)$]	0.0554, 0.0754	0.0871, 0.1776	0.0585, 0.1080
(all data)	0.1129, 0.0887	0.1212, 0.2022	0.1245, 0.1236
peak and hole/eÅ^{-3}	0.788, −0.767	1.141, −1.331	1.114, −0.865

package, and a semiempirical absorption correction was applied by using SADABS.[16] The structures were solved by direct methods and refined by full-matrix least-squares on all F_0^2 data using SHELXS-97[17] and SHELXL-97.[18] All non-H atoms were refined anisotropically, with H atoms bonded to C or N included in calculated positions by using the riding method; those bonded to the water O atoms could not be located. All other calculations were carried out by using the SHELXTL package.[19] Static disorder is shown by the PF_6^- anion in **2**, and by the acetone solvent molecule in 3•Me_2CO. Crystallographic data and refinement details are presented in Table 1.

Hyper-Rayleigh Scattering. The apparatus and experimental procedures used for the fs HRS studies were exactly as described previously.[20] All measurements were carried out in acetonitrile with crystal violet as an external reference (octupolar $\beta_{xxx,800}$ = 500 × 10^{-30} esu in acetonitrile; from the value of 340 × 10^{-30} esu in methanol, corrected for local field factors at optical frequencies), and using the 800 nm fundamental of a regenerative mode-locked Ti^{3+}:sapphire laser (Spectra Physics, model Tsunami, 100 fs pulses, 1 W, 80 MHz). Dilute solutions (10^{-5}–10^{-6} M) were used to ensure a linear dependence of $I_{2\omega}/I_{\omega}^2$ on concentration, precluding the need for Lambert–Beer correction factors. An absence of demodulation at 800 nm, i.e. constant values of β versus frequency, confirmed that no luminescence contributions to the HRS signals were present at 400 nm. The reported β values are the averages taken from measurements at different amplitude modulation frequencies. The β_{800} data shown are based on the assumption of a single β component, and are derived from the total HRS intensity $\langle\beta_{HRS}^2\rangle$ by using eq 1.

$$\langle\beta_{HRS}^2\rangle = \left(\frac{1}{7} + \frac{1}{35}\right)\beta_{800}^2 \tag{1}$$

Unfortunately, due to the use of very low concentrations and the relatively low signal intensities obtained, it was not possible to measure HRS depolarization ratios[21] for the new compounds.

Stark Spectroscopy. The Stark apparatus, experimental methods, and data collection procedure were as previously reported,[22] except that a Xe arc lamp was used as the light source instead of a W filament bulb. The Stark spectrum for each compound was measured at least twice. The data analysis was carried out as previously described,[22] by using the zeroth, first, and second derivatives of the absorption spectrum for analysis of the Stark $\Delta\epsilon(\nu)$ spectrum in terms of the Liptay treatment.[23] The dipole-moment change, $\Delta\mu_{12} = \mu_e - \mu_g$, where μ_e and μ_g are the respective excited and ground-state dipole moments, was then calculated from the coefficient of the second derivative component. Butyronitrile was used as the glassing medium, for which the local field correction f_{int} is estimated as 1.33.[22] A two-state analysis of the ICT transitions gives

$$\Delta\mu_{ab}^2 = \Delta\mu_{12}^2 + 4\mu_{12}^2 \tag{2}$$

where $\Delta\mu_{ab}$ is the dipole-moment change between the diabatic states, and $\Delta\mu_{12}$ is the observed (adiabatic) dipole-moment change. The value of the transition dipole-moment μ_{12} can be determined from the oscillator strength f_{os} of the transition by

$$|\mu_{12}| = \left(\frac{f_{os}}{1.08 \times 10^{-5} E_{max}}\right)^{1/2} \tag{3}$$

where E_{max} is the energy of the ICT maximum (in wavenumbers), and μ_{12} is in eÅ. The latter is converted into Debye units on multiplying by 4.803. The degree of delocalization c_b^2 and electronic coupling matrix element H_{ab} for the diabatic states are given by

$$c_b^2 = \frac{1}{2}\left[1 - \left(\frac{\Delta\mu_{12}^2}{\Delta\mu_{12}^2 + 4\mu_{12}^2}\right)^{1/2}\right] \tag{4}$$

$$|H_{ab}| = \left|\frac{E_{max}(\mu_{12})}{\Delta\mu_{ab}}\right| \tag{5}$$

If the hyperpolarizability β_0 tensor has only nonzero elements along the ICT direction, then this quantity is given by

$$\beta_0 = \frac{3\Delta\mu_{12}(\mu_{12})^2}{(E_{max})^2} \tag{6}$$

dx.doi.org/10.1021/ic500145r | Inorg. Chem. 2014, 53, 3798–3811

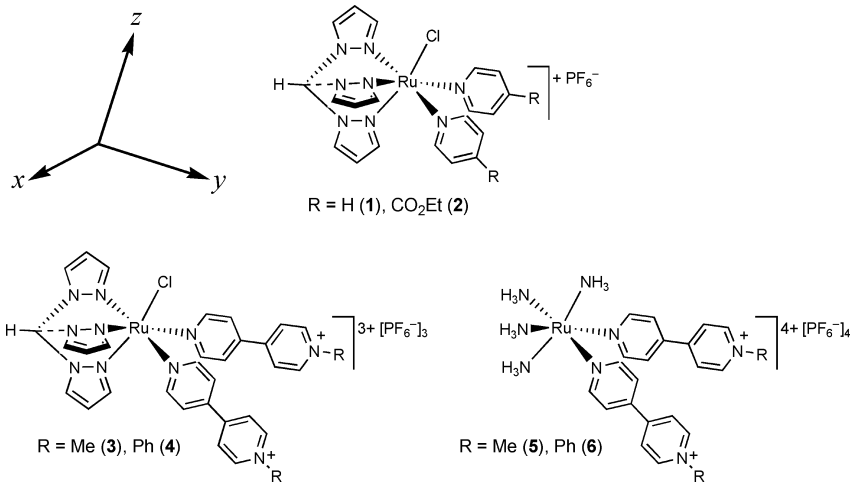

Figure 1. Chemical structures of the new Ru^{II} complex salts investigated, together with related previously reported *cis*-$\{Ru^{II}(NH_3)_4\}^{2+}$ species.[9a] The axes shown approximate to those used in the theoretical studies.

Table 2. UV−Vis and Electrochemical Data for Complex Salts 1−6 in Acetonitrile

				$E_{1/2}$, V vs Ag−AgCl (ΔE_p, mV)[b]	
complex salt	λ_{max}, nm[a] (ε, 10^3 M^{-1} cm^{-1})	E_{max} (eV)	assignment	$Ru^{III/II}$	L^A reductions
1	365 (13.6)	3.40	d → π^*(py)	0.80 (80)	
	282sh (4.1)	4.40	d → π^*(Tpm)		
	246 (7.4)	5.04	π → π^*		
2	423 (14.0)	2.93	d → π^*(EIN)	0.90 (70)	−1.48 (70)
	328sh (4.7)	3.78	d → π^*(EIN)		−1.62 (70)
	293sh (5.2)	4.23	d → π^*(Tpm)		
	266 (9.1)	4.66	π → π^*		
3	499 (12.5)	2.48	d → $\pi^*(MeQ^+)$	0.91 (60)	−0.84 (140)
	333sh (6.4)	3.72	d → π^*(Tpm)		−1.50 (130)
	263 (42.3)	4.71	π → π^*		
4	525 (18.3)	2.36	d → $\pi^*(PhQ^+)$	0.93 (70)	−0.62 (100)
	284 (40.4)	4.37	π → π^*		−1.29 (180)
5[c]	570 (17.5)	2.18	d → $\pi^*(MeQ^+)$	0.79 (85)	−0.81 (110)
	502 (15.1)	2.47	d → $\pi^*(MeQ^+)$		−1.42 (65)
	262 (33.3)	4.73	π → π^*		−1.55 (70)
6[c]	606 (20.4)	2.05	d → $\pi^*(PhQ^+)$	0.79 (70)	−0.66 (110)
	528 (16.5)	2.35	d → $\pi^*(PhQ^+)$		−1.26 (70)
	284 (31.2)	4.37	π → π^*		−1.38 (65)

[a]Solutions ca. $1-7 \times 10^{-5}$ M. [b]Measured in solutions ca. 10^{-3} M in analyte and 0.1 M in $[N(C_4H_9\text{-}n)_4]PF_6$ at a 2 mm disk glassy carbon (**1**−**4**) or Pt (**5** and **6**) working electrode with a scan rate of 100 mV s^{-1} (**1**−**4**) or 200 mV s^{-1} (**5** and **6**). Ferrocene internal reference $E_{1/2}$ = 0.44 V, ΔE_p = 70 mV. [c]Data taken from ref 9a.

A relative error of ±20% is estimated for the β_0 values derived from the Stark data and using eq 5, while experimental errors of ±10% are estimated for μ_{12}, $\Delta\mu_{12}$, and $\Delta\mu_{ab}$, ±15% for H_{ab} and ±50% for c_b^2. Note that the ±20% uncertainty for the β_0 values is merely statistical and does not account for any errors introduced by two-state extrapolation.

Theoretical Calculations. Geometry optimizations (in the gas phase only), density functional theory (DFT), and time-dependent DFT (TD-DFT) calculations were undertaken by using the Gaussian 09 software.[24] Studies were performed by using the functionals B86,[25] B3LYP,[26] CAM-B3LYP,[27] PBE1PBE,[28] or M06,[29] with various basis sets. The complexes in the PF_6^- salts **1**−**4** are denoted **1′**−**4′**. For the monocationic complexes **1′** and **2′**, the best simulations of the experimental UV−vis spectra are obtained with B3LYP and the LANL2DZ[30] basis set for Ru with 6-311G* for C, N, and O; 6-311G for H; and 6-311+G* for Cl. In contrast, the spectra of the tricationic complexes **3′** and **4′** are best modeled with the PBE1PBE functional with the same basis set combination. Using these parameters and the conductor-like polarizable continuum model (CPCM)[31] of acetonitrile, the first 50 excited singlet states were calculated via TD-DFT. UV−vis spectra in the range 200−800 nm were simulated by using the GaussSum program[32] (curve fwhm = 3000 cm^{-1}).

β_0 values were calculated by using B3LYP (for **2′** only) or PBE1PBE (for **2′**−**4′**), as the analytical second derivative of the dipole moment with respect to an external electric field. The LANL2DZ/6-311G/6-311G*/6-311+G* mixed basis set was used, and calculations were run both in the gas phase and in acetonitrile. The calculated β_{tot} value is the overall magnitude of the static first hyperpolarizability related to the individual tensor components according to[33]

$$\beta_{tot} = [(\beta_{xxx} + \beta_{xyy} + \beta_{xzz})^2 + (\beta_{yyy} + \beta_{yzz} + \beta_{yxx})^2 + (\beta_{zzz} + \beta_{zxx} + \beta_{zyy})^2]^{1/2} \quad (7)$$

and

dx.doi.org/10.1021/ic500145r | Inorg. Chem. 2014, 53, 3798−3811

$$\beta_{tot} = (\beta_x^2 + \beta_y^2 + \beta_z^2)^{1/2} \quad (8)$$

For the complexes studied here with C_s point group symmetry, Gaussian 09 assigns the plane of symmetry as *yz*, with the *y* axis directed between the pyridine/pyridyl ligands but offset somewhat from the C_3 axis of the Ru^{II}(Tpm) unit (as shown in Figure 1).

RESULTS AND DISCUSSION

Synthesis. The new complex salts **1**–**3** were prepared from reactions of the precursor $[Ru^{II}Cl_2(Tpm)(NO)]PF_6$[13] in methanol. As in other studies, the linearly coordinated nitrosyl ligand is labilized selectively via nucleophilic attack by azide anion,[34] and one of the chloride ligands is substituted also. Substitution of the remaining chloride occurs much less readily, minimizing the formation of unwanted tris-pyridyl derivatives. **1** and **2** were obtained in reasonably good yields and pure form relatively readily. However, column chromatography on basic alumina with significant sacrifice of product was required in order to isolate pure **3**. Using the same method for **4** did not afford a sufficiently pure material, so this complex was instead prepared from $Ru^{II}Cl_3(Tpm)\bullet 1.5H_2O$[12] in 1:1 ethanol/water, followed by chromatographic purification as for **3**. Initial experiments using silica gel as the column support resulted in decomposition of the complexes. It is worth noting that the mono-MeQ^+ complex salts $[Ru^{II}(Tpm)(L)(MeQ^+)][PF_6]_3$ [L = 2,2′-bipyridyl or 4-methyl-4′-(*N*-phenothiazylmethyl)-2,2′-bipyridyl] have been studied for their photoexcitation properties by Meyer and colleagues.[10c]

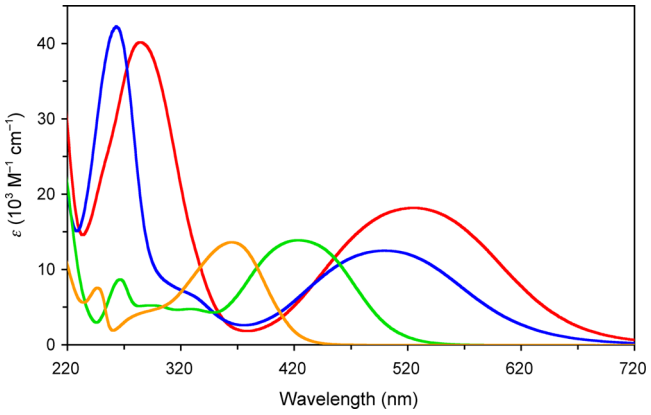

Figure 2. UV–vis absorption spectra of the complex salts **1** (gold), **2** (green), **3** (blue), and **4** (red) in acetonitrile at 293 K.

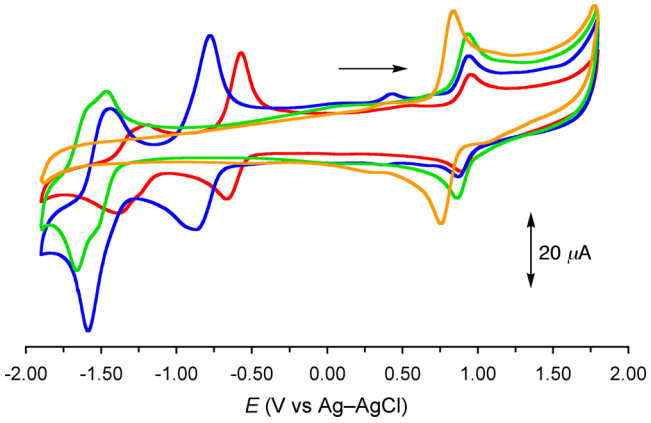

Figure 3. Cyclic voltammograms of the complex salts **1** (gold), **2** (green), **3** (blue), and **4** (red) recorded at 100 mV s^{-1} in acetonitrile (0.1 M in $[N(C_4H_9\text{-}n)_4]PF_6$) with a glassy carbon working electrode. The concentrations are variable in order to decrease overlap between the traces, and the single-headed arrow indicates the direction of the initial scans.

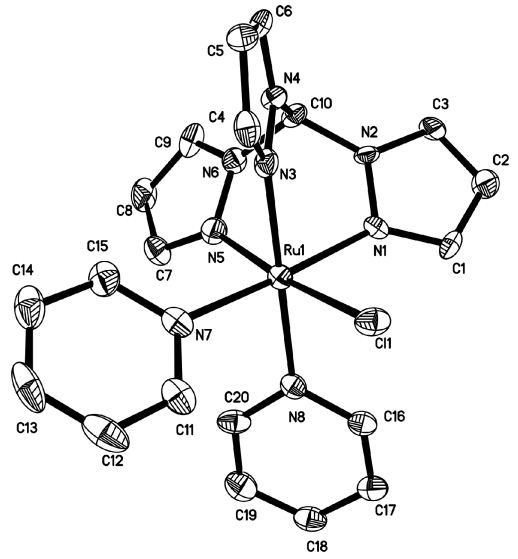

Figure 4. Representation of the molecular structure of the complex cation in the salt **1**•Me_2CO, with the PF_6^- anion, acetone molecule, and H atoms removed for clarity (50% probability ellipsoids).

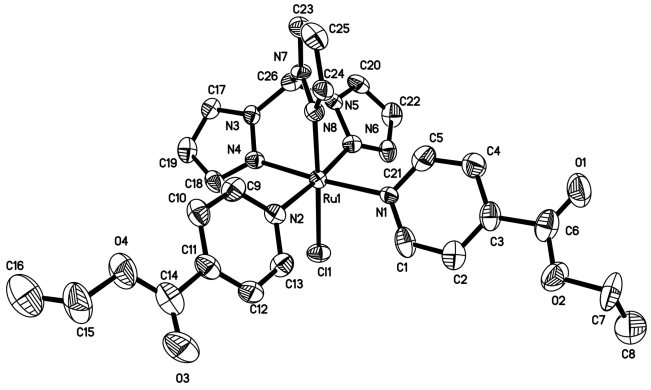

Figure 5. Representation of the molecular structure of the complex cation in the salt **2**, with the PF_6^- anion and H atoms removed for clarity (50% probability ellipsoids).

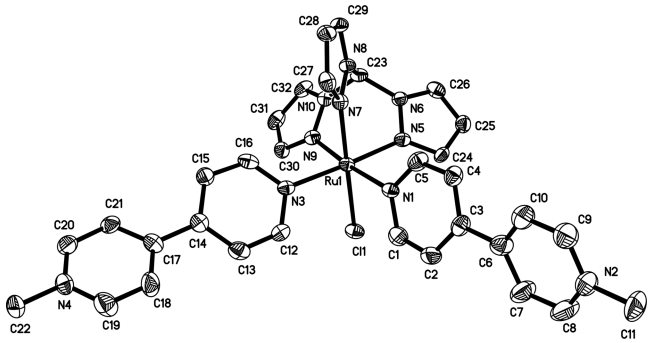

Figure 6. Representation of the molecular structure of the complex cation in the salt **3**•Me_2CO, with the PF_6^- anions, acetone molecule, and H atoms removed for clarity (50% probability ellipsoids).

dx.doi.org/10.1021/ic500145r | Inorg. Chem. 2014, 53, 3798–3811

Table 3. Selected Interatomic Distances (Å) and Angles (deg) for the Complex Salts 1•Me_2CO, 2, and 3•Me_2CO

	1•Me_2CO	2	3•Me_2CO
Ru–Cl	2.398(2)	2.386(2)	2.403(1)
Ru–N(L^A)	2.067(5)	2.100(7)	2.100(4)
Ru–N(L^A)	2.084(5)	2.085(7)	2.077(4)
Ru–N(Tpm, trans-Cl)	2.084(5)	2.022(8)	2.033(4)
Ru–N(Tpm, trans-L^A)	2.048(5)	2.054(7)	2.050(4)
Ru–N(Tpm, trans-L^A)	2.082(4)	2.051(7)	2.055(4)
Cl–Ru–N(L^A)	90.1(1)	91.7(2)	91.2(1)
Cl–Ru–N(L^A)	90.1(1)	90.6(2)	91.1(1)
Cl–Ru–N(Tpm)	94.5(2)	91.5(2)	89.7(1)
Cl–Ru–N(Tpm)	90.1(1)	89.6(2)	89.7(1)
Cl–Ru–N(Tpm)	173.9(1)	175.9(2)	173.8(1)
N(L^A)–Ru–N(L^A)	89.4(2)	95.5(3)	95.7(2)
N(L^A)–Ru–N(Tpm)	176.1(2)	174.6(3)	174.2(2)
N(L^A)–Ru–N(Tpm)	90.6(2)	89.0(3)	87.6(2)
N(L^A)–Ru–N(Tpm)	93.5(2)	91.8(3)	93.6(2)
N(L^A)–Ru–N(Tpm)	94.5(2)	89.7(3)	93.6(2)
N(L^A)–Ru–N(Tpm)	179.8(2)	174.9(3)	176.6(2)
N(L^A)–Ru–N(Tpm)	94.9(2)	91.1(3)	90.0(2)
N(Tpm)–Ru–N(Tpm)	85.5(2)	85.7(3)	86.7(2)
N(Tpm)–Ru–N(Tpm)	86.5(2)	86.8(3)	86.7(2)
N(Tpm)–Ru–N(Tpm)	85.0(2)	86.5(3)	85.1(2)

Table 4. Visible Absorption and HRS Data for Complex Salts 2–6 in Acetonitrile

		(10^{-30} esu)	
complex salt	λ_{max}, nm[a] (ε, 10^3 M^{-1} cm^{-1})	$(\langle\beta^2_{HRS}\rangle)^{1/2}$[b]	β_{800}[c]
2	423 (14.0)	29 ± 3	71 ± 7
3	499 (12.5)	40 ± 5	96 ± 11
4	525 (18.3)	35 ± 4	84 ± 9
5[d]	570 (17.5) 502 (15.1)	58 ± 9	139 ± 21
6[d]	606 (20.4) 528 (16.5)	53 ± 8	127 ± 19

[a]Solutions ca. $1-7 \times 10^{-5}$ M. [b]The total molecular HRS response without any assumption of symmetry or contributing tensor elements, measured by using an 800 nm Ti^{3+}:sapphire laser. The quoted cgs units (esu) can be converted into SI units (C^3 m^3 J^{-2}) by dividing by a factor of 2.693×10^{20}, or into atomic units (au) by dividing by 0.8640×10^{-32}. [c]First hyperpolarizability derived by assuming a single major tensor component. [d]Data taken from ref 9a.

Electronic Spectroscopy. The electronic absorption spectra of the new complex salts **1**–**4** were recorded in acetonitrile, and the results are presented in Table 2, together with data reported previously for **5** and **6**[9a] for comparison purposes. Representative spectra of **1**–**4** are shown in Figure 2. Each of the new complexes shows a single intense, broad absorption band in the visible region, which can be ascribed $d(Ru^{II}) \rightarrow \pi^*(L^A)$ (L^A = EIN, MeQ^+, or PhQ^+) MLCT character. Additional high-energy bands in the UV region are due to intraligand $\pi \rightarrow \pi^*$ excitations.

The MLCT band shows a trend of steady red-shifting on moving along the series **1** → **4** (Figure 2), consistent with an expected increasing electron acceptor strength of L^A. The band intensities are similar for **1**–**3** but a little larger for **4**. The previously reported compounds **5** and **6** show MLCT bands with two distinct maxima,[9a] while the related **3** and **4** display very broad bands with only one, quite poorly defined maximum. However, TD-DFT calculations (see below) confirm the expectation that multiple transitions contribute to these bands. It is probably coincidental that the maxima estimated for **3** and **4** correspond closely with the respective high energy maxima for **5** and **6**. The fact that the latter show also MLCT transitions to significantly lower energies indicates that a *cis*-$\{Ru^{II}(NH_3)_4\}^{2+}$ center is more strongly electron-donating than a $\{Ru^{II}Cl(Tpm)\}^+$ moiety. The constant positions of the UV bands on replacing the Tpm and chloride with four ammonia ligands indicates that these absorptions are associated with the MeQ^+/PhQ^+ ligands primarily, the weaker bands due to Tpm being masked in **3** and **4**.

Electrochemistry. The complex salts **1**–**4** were studied by cyclic voltammetry in acetonitrile, and the results are presented in Table 2, together with data reported previously for **5** and **6**.[9a] Representative voltammograms of **1**–**4** are shown in Figure 3. All of the new complexes show reversible $Ru^{III/II}$ oxidation waves, together with two or more L^A-based reduction processes for **2**–**4** that are quasireversible or irreversible. All of these complexes therefore have the potential to behave as redox-switchable NLO chromophores.[35]

Complex salt **2** shows two overlapping L^A-based reduction waves (Figure 3) that are well resolved by differential pulse measurements. By analogy with **5** and **6**,[9a] the reduction waves for **3** and **4** are expected to correspond with two-electron processes (for the two ligands becoming reduced at very similar potentials), but differential pulse experiments did not resolve these. The $Ru^{III/II}$ potential increases by 100 mV on moving from **1** to **2**, attributable to the electron-withdrawing influence of the two ester substituents. On moving along the series to **3**, then **4**, the $Ru^{III/II}$ waves show

Table 5. Absorption and Stark Spectroscopic Data for Complex Salts 2–6 in Butyronitrile at 77 K[a]

complex salt	λ_{max} (nm)	E_{max} (eV)	f_{os}[b]	μ_{12}[c] (D)	$\Delta\mu_{12}$[d] (D)	$\Delta\mu_{ab}$[e] (D)	r_{12}[f] (Å)	r_{ab}[g] (Å)	c_b^2[h]	H_{ab}[i] (10^3 cm^{-1})	β_0[j] (10^{-30} esu)
2	431	2.88	0.32	5.4	13.6	17.4	2.8	3.6	0.11	7.3	62
3	518	2.39	0.44	7.0	17.5	22.5	3.7	4.7	0.11	6.0	182
4	554	2.24	0.62	8.6	20.7	26.9	4.3	5.6	0.12	5.8	356
5[k]	628	1.98	0.34	6.7	10.1	16.8	2.1	3.5	0.20	6.4	137 (199)
	518	2.39	0.24	5.2	11.3	15.3	2.4	3.2	0.13	6.5	62
6[k]	632	1.96	0.41	7.4	13.8	20.3	2.9	4.2	0.16	5.8	231 (273)
	512	2.42	0.20	4.6	9.9	13.5	2.1	2.8	0.13	6.7	42

[a]The data for **5** and **6** are for the two fitted Gaussian components. [b]For **2**–**4**, obtained from $(4.32 \times 10^{-9}$ M $cm^2)A$ where A is the numerically integrated area under the absorption peak; for **5** and **6**, obtained from $(4.60 \times 10^{-9}$ M $cm^2)\varepsilon_{max} \times$ fwhm where ε_{max} is the maximal molar extinction coefficient and fwhm is in wavenumbers. [c]Calculated from eq 3. [d]Calculated from $f_{int}\Delta\mu_{12}$ using f_{int} = 1.33. [e]Calculated from eq 2. [f]Delocalized electron-transfer distance calculated from $\Delta\mu_{12}/e$. [g]Effective (localized) electron-transfer distance calculated from $\Delta\mu_{ab}/e$. [h]Calculated from eq 4. [i]Calculated from eq 5. [j]Calculated from eq 6; the total values are given in brackets for **5** and **6**. [k]Data taken from ref 9a.

dx.doi.org/10.1021/ic500145r | Inorg. Chem. 2014, 53, 3798–3811

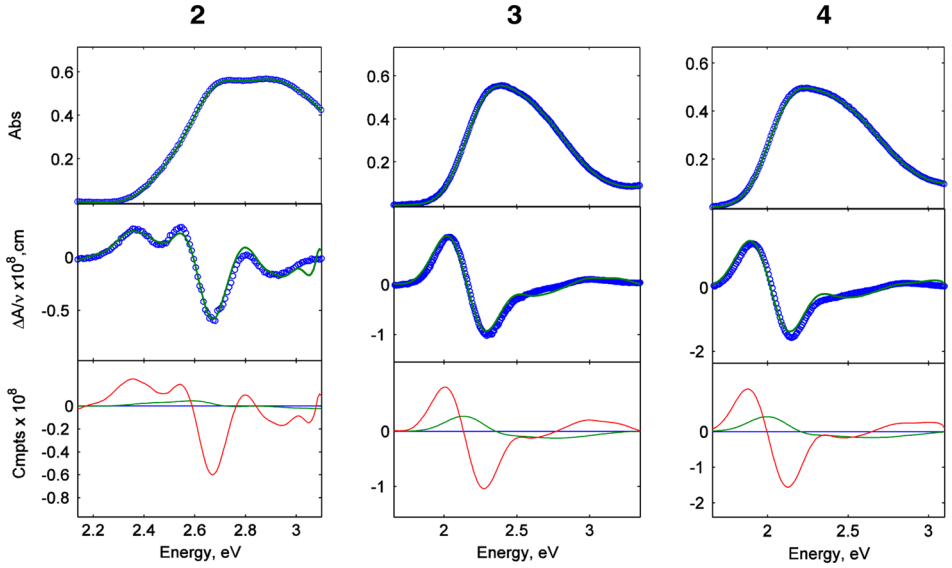

Figure 7. Spectra and calculated fits for the salts **2**–**4**. Top panel: absorption spectrum; middle panel: electroabsorption spectrum, experimental (blue) and fits (green) according to the Liptay equation;[23a] bottom panel: contribution of 0th (blue), first (green), and second (red) derivatives of the absorption spectrum to the calculated fits.

only small further anodic shifts, indicating that the energy of the Ru-based HOMO is affected only slightly by changing the 4-substituent on the pyridyl ligands. The stronger electron-accepting ability of PhQ^+ as opposed to MeQ^+, noted previously,[9a,15,36] increases the potentials for L^A-based reductions on moving from **3** to **4** (Figure 3).

Comparing the data for **3** and **4** with those for **5** and **6** reveals that the $Ru^{III/II}$ potentials decrease by 120–140 mV when ammonia ligands replace Tpm and chloride (Table 2). This observation is consistent with the corresponding decreases in the MLCT energies (see above). As expected, the L^A-based reduction waves are comparatively less sensitive to changes in the coligands, with (inconsistent) changes of only 30–40 mV for the $E_{1/2}$ value of the first wave on moving from **3** to **5** or from **4** to **6**.

Crystallography. Single crystal X-ray structures have been obtained for the complex salts **1**•Me_2CO, **2**, and **3**•Me_2CO. Representations of the molecular structures are shown in Figures 4, 5, and 6, and selected interatomic distances and angles are presented in Table 3.

The structures reveal the expected tridentate, facially coordinating mode of the Tpm ligand. Each of the complexes adopts a slightly distorted octahedral geometry, with N(Tpm)–Ru–N(Tpm) angles of ca. 85–87°, and small deviations from the ideal 90 or 180° in most of the other angles (Table 3). The structure of the complex in **1**•Me_2CO resembles closely that reported for $[Ru^{II}(Tpm)(py)_3][PF_6]_2$.[37] In **2** and **3**•Me_2CO, the Ru–N(Tpm) distances are shorter than the Ru–N(L^A) distances by ca. 0.04–0.08 Å, while this is not the case for **1**•Me_2CO. Also, while the Ru–N(Tpm) distances trans to the L^A ligands are slightly longer than those trans to the chloride ligand in **2** and **3**•Me_2CO, such an apparent structural trans effect is not observed in **1**•Me_2CO.

In **1**•Me_2CO, the dihedral angles formed between the planes of the py ligands and their opposite pyrazolyl (pyz) rings are very different, being 12.6 and 89.0°. In contrast, the angles between the pyridyl and trans pyz rings in **2** are both small and closely similar (7.0 and 9.0°). An intermediate degree of variation is found in **3**•Me_2CO, with corresponding angles of 8.7 and 25.5°. The dihedral angles between the two pyridyl rings within the MeQ^+ ligands in **3**•Me_2CO are both 25.3°, similar to those observed in related complexes previously.[9b,34e]

While various Ru^{II}(Tpm) complexes have been structurally characterized,[10b,d–q,s,37] **2** appears to be only the second Ru^{II} complex of the EIN ligand for which crystallographic data are available, following *trans*-(Cl,CO)(P,P)-$Ru^{II}Cl(CH{=}CH^nBu)(PPh_3)_2$(EIN)(CO).[38] The ester substituents in **2** lie almost coplanar with the pyridyl rings, forming dihedral angles of 6.4 and 9.1°, the latter being identical to that observed in *trans*-(Cl,CO)(P,P)-$Ru^{II}Cl(CH{=}CH^nBu)(PPh_3)_2$(EIN)(CO).[38] All of **1**•Me_2CO, **2**, and **3**•Me_2CO adopt centrosymmetric packing structures, so none of these materials is expected to show significant quadratic NLO effects.

Hyper-Rayleigh Scattering. The β values of complex salts **2**–**4** have been measured in acetonitrile solutions by using the HRS technique with a 800 nm laser,[20] and the results are collected in Table 4, together with the data published previously for **5** and **6**.[9a] **1** did not give a significant HRS signal, consistent with its relatively high energy absorption bands (see above) being associated with only a small NLO response. The fundamental wavelength was chosen because none of the complexes absorbs significantly at 800 nm, and only **2** absorbs relatively strongly at the second harmonic (SH) of 400 nm (Figure 2).

The β_{800} values obtained for **5** and **6** are surprising in not showing an increase in the NLO response as the electron-accepting strength of the pyridinium units increases.[9a] These data contrast with the results of earlier 1064 nm HRS studies on 1D dipolar Ru^{II} ammine complexes, which always show substantial increases in β_0 on replacing a Me with Ph *N*-substituent.[15,36,39] It is noteworthy that the HRS data for the new compounds **3** and **4** are reminiscent of those for **5** and **6** (Table 4), showing responses that are not significantly different. The significant increases in β_{800} on moving from **3** to **5** or from **4** to **6** are consistent with the stronger electron-donating power of a *cis*-$\{Ru^{II}(NH_3)_4\}^{2+}$ as opposed to a $\{Ru^{II}Cl(Tpm)\}^+$ moiety, indicated by the MLCT absorption

dx.doi.org/10.1021/ic500145r | Inorg. Chem. 2014, 53, 3798–3811

Table 6. Selected TD-DFT-Calculated and Experimental Data for the Complexes 1′−4′[a]

complex	λ_{exp}[b] (nm)	λ_{max}[c] (nm)	λ_{calc} (nm)	E_{calc} (eV)	f_{os}	major contributions (weight)[d]
1′	365	354	356	3.48	0.17	H−1 → L (54%); H−1 → L+1 (11%); H → L+1 (24%)
			354	3.50	0.15	H−1 → L+1 (75%); H → L+1 (14%)
			335	3.71	0.05	H−2 → L (82%)
			290	4.27	0.05	H−1 → L+3 (20%); H → L+2 (12%); H → L+5 (21%); H → L+7 (13%)
			278	4.46	0.03	H−1 → L+7 (13%); H → L+7 (64%); H → L+8 (15%)
			278	4.47	0.03	H−1 → L+7 (74%); H−1 → L+8 (11%)
			234	5.30	0.03	H−3 → L+1 (93%)
			224	5.54	0.05	H−7 → L (17%); H−6 → L+1 (55%)
2′	423	424	436	2.84	0.20	H−1 → L (93%)
			424	2.92	0.14	H−2 → L+1 (16%); H−1 → L+1 (72%)
			396	3.13	0.05	H−2 → L (97%)
			393	3.16	0.12	H−2 → L+1 (81%); H−1 → L+1 (12%)
			323	3.83	0.03	H−1 → L+2 (45%); H → L+8 (34%)
			317	3.92	0.02	H−2 → L+2 (10%); H−2 → L+6 (23%); H → L+3 (42%); H → L+8 (12%)
			291	4.26	0.08	H−2 → L+2 (13%); H−1 → L+2 (23%); H → L+3 (21%); H → L+5 (17%)
			274	4.53	0.04	H → L+7 (75%); H → L+8 (18%)
			253	4.89	0.06	H−6 → L (85%)
3′	499	505	515	2.41	0.34	H−1 → L (86%); H → L+1 (12%)
			487	2.55	0.16	H−1 → L+1 (82%)
			450	2.76	0.05	H−2 → L (96%)
			444	2.79	0.06	H−2 → L+1 (89%)
			310	4.01	0.06	H−1 → L+4 (12%); H → L+5 (25%); H → L+12 (19%)
			308	4.03	0.05	H−1 → L+4 (63%); H → L+5 (15%)
			298	4.16	0.03	H−1 → L+8 (11%); H → L+5 (29%); H → L+12 (23%)
			297	4.18	0.05	H−4 → L (77%); H−1 → L+6 (17%)
			290	4.28	0.07	H−5 → L (22%); H−4 → L+1 (21%); H−1 → L+9 (23%)
			260	4.77	0.30	H−8 → L (64%)
			257	4.83	0.12	H−8 → L+1 (47%); H → L+11 (21%)
4′	525	525	536	2.32	0.39	H−1 → L (89%)
			506	2.45	0.17	H−1 → L+1 (82%)
			464	2.67	0.06	H−2 → L (97%)
			458	2.71	0.07	H−2 → L+1 (91%)
			314	3.95	0.25	H−5 → L+1 (12%); H−4 → L (14%); H → L+5 (34%)
			313	3.96	0.14	H−1 → L+4 (39%); H → L+5 (21%)

[a]All calculations used the LANL2DZ/6-311G/6-311G*/6-311+G* mixed basis set, with the B3LYP functional for 1′ and 2′, but PBE1PBE for 3′ and 4′. Only the main transitions within each band are included. [b]λ_{max} value for lowest energy band measured with 1−4 in acetonitrile. [c]λ_{max} value derived from the simulated absorption spectrum. [d]H = HOMO, L = LUMO.

and $Ru^{III/II}$ potentials (see above). While caution should be exercised when comparing β values that are uncorrected for resonance, the extent of absorption at 800 and 400 nm is similar, and relatively low for all of **3**−**6**. The β_{800} value for **2** is a little smaller than that of **3**, indicating an actually considerable decrease for the complex with shorter L^A ligands, masked by strong resonance enhancement at 400 nm.

Although the β_{800} data shown are based on the assumption of a single β component, the electronic structures and therefore hyperpolarizabilities of these C_{2v} symmetric complexes must inevitably show substantial 2D character. However, it was unfortunately not possible to measure HRS depolarization ratios for **2**−**4** to assess the relative importance of individual β tensor components.

Stark Spectroscopy. Complex salts **2**−**4** have been studied by Stark spectroscopy[22,23] in butyronitrile glasses at 77 K, and the results are shown in Table 5, together with the data reported already for **5** and **6**.[9a] **1** was not studied because it lacks a visible absorption band, and the operational cutoff of our Stark spectrometer is ca. 370 nm. The latter factor also means that the ILCT absorptions of **2**−**6** could not be analyzed, but these high energy transitions are not in any case expected to contribute to the NLO responses substantially.

The absorption spectra for **5** and **6** were subjected to Gaussian deconvolution in order to allow satisfactory fitting of the Stark data.[9a] Representative absorption and electroabsorption spectra for **2**−**4** are shown in Figure 7. In contrast to the spectra measured in acetonitrile at 293 K (Figure 2), the MLCT bands become asymmetric in frozen glasses, but good fits were nonetheless obtained for these new compounds without deconvolution.

On moving along the series **2** → **4**, the MLCT band shows increasing red-shifts of 0.05, 0.09, and 0.12 eV on going from acetonitrile solution to butyronitrile glass (Tables 2 and 5). Such behavior is typical of Ru^{II} complex salts. At 77 K, the band intensity increases steadily on moving from **2** to **4**, as shown by the values of f_{os} and μ_{12}. As expected, the parameters $\Delta\mu_{12}$, r_{12}, $\Delta\mu_{ab}$, and r_{ab} all increase as L^A becomes larger on moving from **2** to **4**. While the degree of delocalization (represented by c_b^2) remains essentially constant, the matrix element H_{ab} that quantifies the strength of π-electronic coupling decreases as the ligands extend.

dx.doi.org/10.1021/ic500145r | Inorg. Chem. 2014, 53, 3798−3811

Table 7. TD-DFT-Calculated Orbital Energies for the Complexes 1′−4′[a]

orbital	1′	2′	3′	4′
L+12			−0.01	−0.87
L+11			−0.41	−0.97
L+10			−0.53	−0.97
L+9			−1.03	−1.04
L+8	−0.14	−0.27	−1.10	−1.14
L+7	−0.52	−0.58	−1.16	−1.17
L+6	−0.69	−0.81	−1.28	−1.30
L+5	−0.82	−0.99	−1.39	−1.52
L+4	−1.05	−1.23	−1.44	−1.53
L+3	−1.16	−1.25	−1.84	−1.90
L+2	−1.19	−1.27	−1.85	−1.91
L+1	−1.57	−2.43	−3.22	−3.35
L	−1.62	−2.46	−3.28	−3.40
H	−5.76	−5.89	−6.28	−6.28
H−1	−5.78	−5.93	−6.30	−6.31
H−2	−6.17	−6.31	−6.71	−6.72
H−3	−7.52	−7.61	−8.02	−8.02
H−4	−7.58	−7.62	−8.04	−8.02
H−5	−7.66	−7.76	−8.24	−8.11
H−6	−7.74	−7.89	−8.35	−8.13
H−7	−7.89	−8.05	−8.57	−8.17
H−8			−8.60	−8.17

[a]All calculations used the LANL2DZ/6-311G/6-311G*/6-311+G* mixed basis set, with the B3LYP functional for **1′** and **2′**, but PBE1PBE for **3′** and **4′**. H = HOMO, L = LUMO.

We have used the standard two-state model[40] (i.e., eq 6, corresponding with the "perturbation series" convention) to estimate β values, and the results are included in Table 5. This approach is clearly only an approximation due to the two-dimensional nature of the chromophores, and the fact that the MLCT bands of **2**−**4** comprise multiple transitions. It is worth noting that we have found using a Gaussian deconvolution approach (as for **5** to **6**) usually gives total β_0 values similar to those obtained by using direct fitting to the absorption spectra.[9b,41]

The β values show a clear trend of increasing by a total of ca. 6-fold on moving from **2** to **4**. This trend arises from a combination of increasing μ_{12} and $\Delta\mu_{12}$ values, accompanied by decreasing E_{max}. Notably, a different pattern is shown by the HRS β_{800} data (Table 4). The Stark-based β response of **2** is relatively modest, in keeping with its short π-conjugation length and the presence of mildly electron-accepting ester substituents. However, the β values derived for **3** and **4** are large and similar to those which we obtained for the related **5** and **6** by using the same approach previously.[9a] As a further comparison, a β value of 236 × 10^{-30} esu was determined from Stark data obtained under the same conditions for the benchmark organic salt (*E*)-4′-(dimethylamino)-*N*-methyl-4-stilbazolium hexafluorophosphate.[42] The data for **5** and **6** do appear to show an increase in β on replacing the *N*-Me with Ph substituents, but the difference is within the estimated experimental error limits. Also, no clear trend is evident on replacing the chloride and Tpm ligands with NH_3, in contrast to the MLCT absorption, electrochemical, and HRS data (see above).

Density Functional Theory. In order to rationalize the experimental UV−vis spectra, TD-DFT calculations were performed on the complexes **1′**−**4′** by using Gaussian 09.[24]

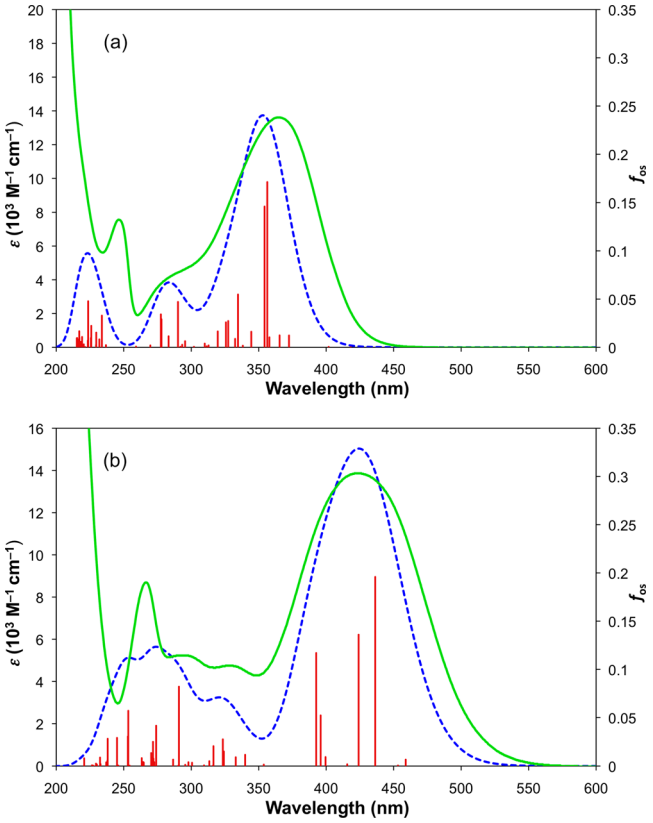

Figure 8. B3LYP/LANL2DZ/6-311G/6-311G*/6-311+G*-calculated (blue) UV−vis spectra of (a) **1′** and (b) **2′**, and the corresponding experimental data (green). The ε-axes refer to the experimental data only, and the vertical axes of the calculated data are scaled to match the main experimental absorptions. The oscillator strength axes refer to the individual calculated transitions (red).

Calculated $S_0 \rightarrow S_1$ transition energies and the corresponding major orbital contributions are presented in Table 6, and frontier orbital energies are presented in Table 7. The simulated spectra are shown together with those measured in Figures 8 and 10.

The lowest energy (LE) and most intense band of **1′** is modeled about three main transitions (Figure 8a) of predominantly HOMO−1 → LUMO, HOMO−1 → LUMO+1, and HOMO−2 → LUMO character (in order of increasing energy). Of the four complexes studied, **1′** is unique in that numerous weak transitions (f_{os} < 0.05) in the region 310−375 nm also contribute to this band. The orbitals involved in the main transitions contained within this band are shown in Figure 9a, while all the other orbitals mentioned in Table 6 are in the Supporting Information (Figure S1). The HOMO, HOMO−1, and HOMO−2 are derived primarily from the Ru d_{yz}, d_{xz}, and $d_{x^2-y^2}$ orbitals, respectively. Each of these also has a significant Cl p orbital contribution, while the HOMO and HOMO−1 also feature a minor component from the Tpm π-orbitals. The LUMO and LUMO +1 both have py π^* character, and the former exhibits also a significant contribution from the two pyz rings trans to the py ligands. Therefore, the calculations confirm the MLCT assignment of the lowest energy band but reveal also a minor LLCT component originating from the Cl. The high energy shoulder at ca. 280 nm (Table 2) is attributable to transitions of largely MLCT character also, but involving π^*-orbitals associated with the Tpm ligand. The LUMO+2 and

dx.doi.org/10.1021/ic500145r | Inorg. Chem. 2014, 53, 3798−3811

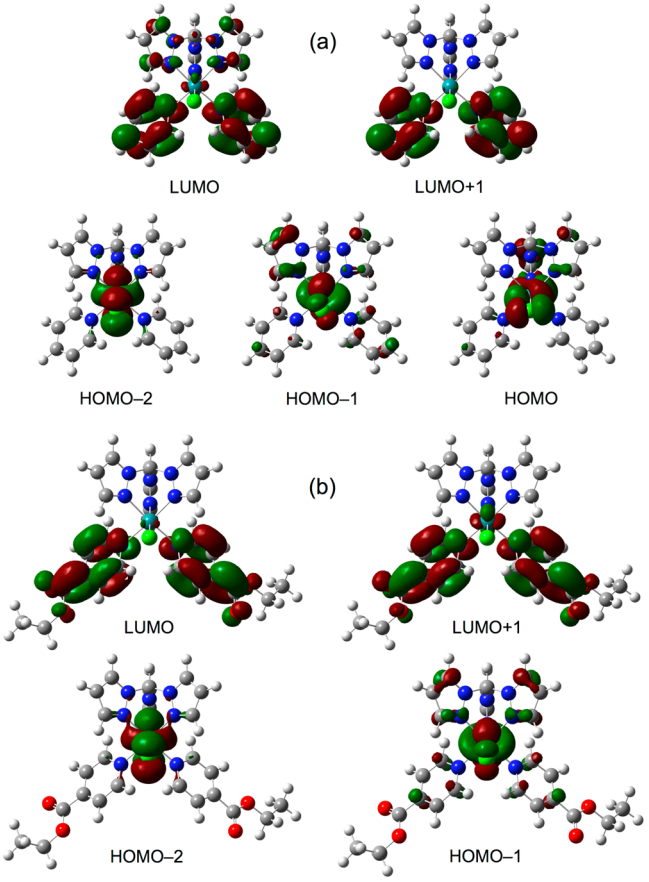

Figure 9. B3LYP/LANL2DZ/6-311G/6-311G*/6-311+G*-derived contour surface diagrams of the MOs involved in the dominant low energy electronic transitions for (a) **1′** and (b) **2′** (isosurface value 0.03 au).

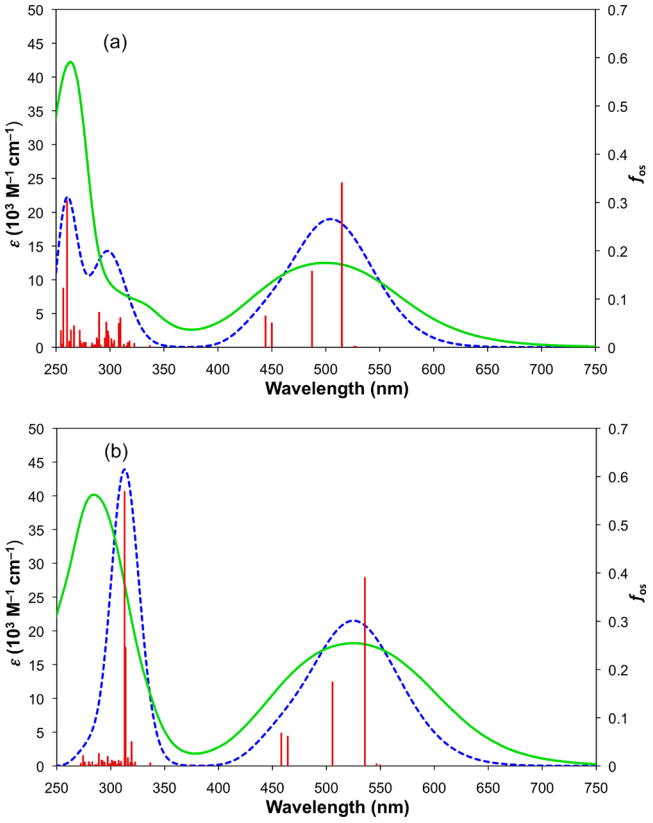

Figure 10. PBE1PBE/LANL2DZ/6-311G/6-311G*/6-311+G*-calculated (blue) UV−vis spectra of (a) **3′** and (b) **4′**, and the corresponding experimental data (green). The ε-axes refer to the experimental data only, and the vertical axes of the calculated data are scaled to match the main experimental absorptions. The oscillator strength axes refer to the individual calculated transitions (red).

LUMO+3 are located on the pyz rings trans to the Cl^- or py ligands, respectively, while LUMO+7 involves all three pyz rings. As expected, the high energy transitions (λ < 250 nm) have intraligand, especially py, $\pi \rightarrow \pi^*$ character.

The LE band of **2′** is derived from four main transitions (Figure 8b) of character comparable to those for **1′**. The orbitals involved in the main transitions contained within the LE band for **2′** are shown in Figure 9b, while all the other orbitals mentioned in Table 6 are in the Supporting Information (Figure S2). The electron-withdrawing ester groups cause the LUMO and LUMO+1 to be stabilized significantly, by 0.84 and 0.86 eV, respectively, relative to **1′** (Table 7). The HOMO, HOMO−1, and HOMO−2 show smaller accompanying relative stabilizations of 0.13−0.15 eV, as the Ru center becomes less electron-rich.

As observed experimentally, the higher energy region of the absorbance spectrum of **2′** is relatively complex and is modeled about many, mostly weak transitions. Those in the region 275−350 nm can be assigned to MLCT directed toward both the EIN and Tpm ligands, while those below 275 nm have mainly EIN $\pi \rightarrow \pi^*$ character.

Calculations on the complexes **3′** and **4′** with B3LYP do not model the LE band accurately, giving bathochromic shifts of ca. 40 nm when compared to the experimental data. Much better results are obtained by using instead the PBE1PBE functional, although this approach overestimates the LE band energies for **1′** and **2′**.

The spectra of **3′** and **4′** both exhibit very broad, LE bands that are modeled almost exclusively about four transitions of largely MLCT character. The orbitals involved in the main transitions contained within these bands are shown in Figures 11a and 11b, respectively, while the other orbitals mentioned in Table 6 are in the Supporting Information (Figures S3 and S4). The nature of the HOMO, HOMO−1, and HOMO−2 remains constant within the series **1′**−**4′**. For **3′** and **4′**, the LUMO and LUMO+1 are π^*-orbitals of the 4,4′-bipyridyl units, weighted slightly in favor of the pyridinium rings. In a qualitative sense, the MO picture derived for these compounds resembles that reported previously for the related tetraammine complexes **5′** and **6′** (from gas-phase B3P86/LANL2DZ calculations that lack quantitative accuracy).[9] On moving from **3′** to **4′**, the LUMO and LUMO+1 are stabilized by 0.12−0.13 eV (Table 7) due to the mild electron-withdrawing influence of the Ph substituents. Because the energies of the donor orbitals are almost constant, the bathochromic shift in the absorption band is attributable primarily to the increased electron-accepting ability of the PhQ^+ ligands with respect to MeQ^+. This conclusion is consistent with the electrochemical data (see above).

The highest energy band in **3′** comprises numerous transitions of mixed LLCT/ILCT character, directed toward the pyridinium moieties. These transitions originate from a combination of π-orbitals located on Tpm and the pyridyl rings of the MeQ^+ ligands as well as a contribution from the

dx.doi.org/10.1021/ic500145r | Inorg. Chem. 2014, 53, 3798−3811

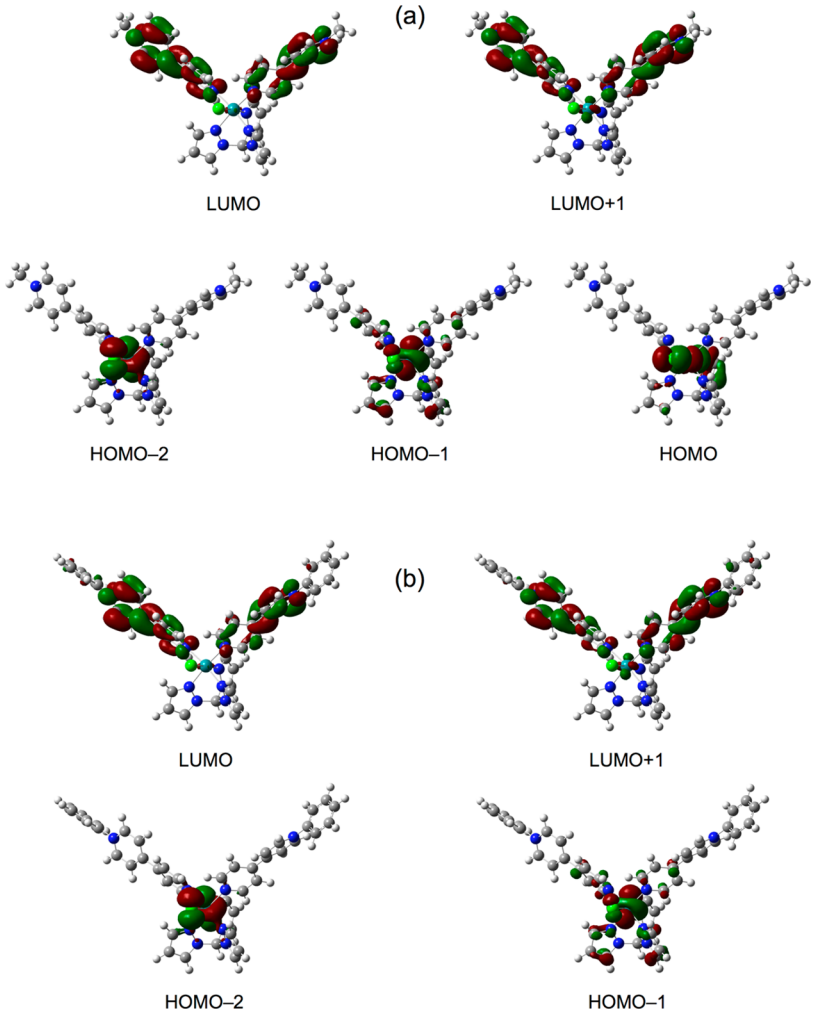

Figure 11. PBE1PBE/LANL2DZ/6-311G/6-311G*/6-311+G*-derived contour surface diagrams of the MOs involved in the dominant low energy electronic transitions for (a) **3′** and (b) **4′** (isosurface value 0.03 au).

Table 8. First Hyperpolarizabilities (10^{-30} esu) Calculated via DFT for the Complexes 1′−4′[a]

complex	functional	β_{xxx}	β_{xxy}	β_{xyy}	β_{yyy}	β_{xxz}	β_{xyz}	β_{yyz}	β_{xzz}	β_{yzz}	β_{zzz}	β_x	β_y	β_z	β_{tot}
2′[b]	B3LYP	−16.9	66.8	8.95	39.3	6.60	−8.79	3.38	0.38	−3.62	13.1	−7.57	102	23.1	105
2′[c]	B3LYP	−5.81	23.7	3.27	11.4	2.06	−2.94	1.28	0.62	−2.44	6.88	−1.92	32.7	10.2	34.3
2′[b]	PBE1PBE	−14.6	59.8	7.92	34.3	5.33	−7.69	2.66	0.40	−3.37	11.7	−6.23	90.7	19.7	93.0
2′[c]	PBE1PBE	−5.07	21.3	2.85	9.99	1.65	−2.58	0.99	0.54	−2.13	6.10	−1.68	29.1	8.73	30.5
3′[b]	PBE1PBE	−0.48	217	1.59	82.1	21.3	−0.07	8.75	0.98	−4.35	10.4	2.10	295	40.4	298
3′[c]	PBE1PBE	2.10	211	2.68	68.1	19.8	0.19	7.15	0.47	−1.62	4.57	5.25	277	31.5	279
4′[b]	PBE1PBE	6.66	254	1.42	96.3	18.2	−0.38	7.80	1.55	−4.64	10.6	9.64	346	36.7	348
4′[c]	PBE1PBE	9.44	197	2.25	59.7	13.8	−0.31	5.08	0.68	−1.99	4.75	12.4	255	23.7	256

[a]All calculations used the LANL2DZ/6-311G/6-311G*/6-311+G* mixed basis set. [b]In acetonitrile. [c]In the gas phase.

Cl^- ligand. The intermediate energy band at ca. 300 nm includes transtions of MLCT character dircted toward the Tpm ligand. The intense band at ca. 285 nm in **4′** is primarily based on two intense transitions of mixed LLCT/ILCT character, involving PhQ^+ π^*-orbitals that include a minor contribution from the Ph substituent.

The results of β_0 calculations on **2′**−**4′** are shown in Table 8. Using either B3LYP or PBE1PBE for **2′** gives broadly similar results, with $\beta_{tot} \approx 100 \times 10^{-30}$ esu in acetonitrile. Calculations conducted in the gas phase afford consistently smaller values for β_{tot} and all individual β components when compared with acetonitrile solution. A similarly large solvation effect has been observed with mono- and bimetallic Ru^{II} ammine complexes treated at the B3LYP level of theory.[43] Given the axis convention adopted in the calculations (Figure 1; see also the Supporting Information, Figure S5), β_y dominates, and β_{xxy} is the most significant of the "off-diagonal" tensor components.

For **3′** and **4′**, again including the solvent increases β_{tot} with respect to the gas phase, but the difference is relatively small for **3′**. Interestingly, β_{tot} increases substantially on moving from **3′** to **4′** in acetonitrile, but a corresponding slight decrease is predicted in the gas phase. Clearly, the data calculated in solution are expected to best model the

dx.doi.org/10.1021/ic500145r | Inorg. Chem. 2014, 53, 3798−3811

measured parameters, and when using PBE1PBE in each case, β_{tot} (10^{-30} esu) increases from ca. 100 for **2′** to ca. 300 for **3′**, then ca. 440 for **4′**. These predictions agree relatively well with the β_0 values determined via Stark spectroscopy (Table 5), indicating that the HRS measurements give a less reliable indication of the NLO responses for these complexes. It is also worth noting that previous finite-field calculations on **5′** and **6′** predict that the total β_0 value increases (by ca. 30%) when the Me substituents are replaced with Ph.[9b] When compared with **2′**, the π-conjugated molecular frameworks of **3′** and **4′** are extended along the y direction, so the relative dominance of the β_y and β_{xxy} terms increases.

CONCLUSION

We have synthesized and characterized several new Ru^{II}(Tpm) complexes. Their UV−vis absorption spectra are dominated by intense, single-maximum MLCT bands, the energies of which correlate with the electron-accepting ability of the pyridine/pyridyl (L^A) ligands. The $Ru^{III/II}$ oxidation waves measured by cyclic voltammetry in acetonitrile are reversible, with $E_{1/2}$ covering a range of 0.80−0.93 V vs Ag−AgCl, while the ligand-based reduction potentials show larger variations. Single crystal X-ray structures have been determined for three complex salts, revealing centrosymmetric packing structures. The values of β_{800} measured via the HRS technique in acetonitrile are relatively large but show little dependence on L^A. In contrast, the β_0 values estimated from Stark spectroscopic data measured for the lowest energy absorption bands in butyronitrile at 77 K increase substantially with the electron-accepting strength of L^A. TD-DFT calculations confirm that the latter bands have largely $Ru^{II} \rightarrow L^A$ MLCT character, while $Ru^{II} \rightarrow$ Tpm MLCT transitions occur at higher energies. β_0 values predicted via DFT concur with the Stark measurements, showing large increases as L^A becomes more electron deficient. Comparisons with the experimental data reported previously for related complexes do not show clearly whether a *cis*-$\{Ru^{II}(NH_3)_4\}^{2+}$ or $\{Ru^{II}Cl(Tpm)\}^{+}$ center gives larger NLO responses. However, the greater electron-richness at the metal imparted by having ammine ligands is apparent from the MLCT absorption and electrochemical data.

ASSOCIATED CONTENT

Supporting Information

Crystallographic information in CIF format; Cartesian coordinates of theoretically optimized geometries for the complexes **1′**−**4′**; additional MO figures and depictions of axis convention used in the calculations. This material is available free of charge via the Internet at http://pubs.acs.org.

AUTHOR INFORMATION

Corresponding Author

*E-mail: b.coe@manchester.ac.uk.

Notes

The authors declare no competing financial interest.

ACKNOWLEDGMENTS

We thank the EPSRC for support (grant EP/G02099) and also the Fund for Scientific Research-Flanders (FWO-V, G.0312.08) and the University of Leuven (GOA/2011/03). B.S.B. acknowledges the Beckman Institute of the California Institute of Technology for support. We are grateful to James Amphlett (Manchester) for assistance with the purification of complex salt **3** and to Nick Van Steerteghem (Leuven) for help with the HRS experiments.

REFERENCES

(1) (a) Bennett, M. A.; Bruce, M. I.; Cifuentes, M. P.; Deeming, A. J.; Haines, R. J.; Hill, A. F.; Humphrey, M. G.; Khan, K.; Pomeroy, R. K.; Sappa, E.; Smith, A. K.; Wenger, E. In *Comprehensive Organometallic Chemistry II*; Abel, E. W., Stone, F. G. A., Wilkinson, G., Eds.; Pergamon Press: Oxford, U.K., 1995; Vol. *7*, pp 291−960. (b) Che, C.-M.; Housecroft, C. E.; Lau, T.-C. In *Comprehensive Coordination Chemistry II*; McCleverty, J. A., Meyer, T. J., Eds.; Pergamon Press: Oxford, U.K., 2004; Vol. *5*, pp 555−847. (c) Butler, I. R.; Cadierno, V.; Cifuentes, M. P.; Crochet, P.; Dyson, P. J.; Gimeno, J.; Humphrey, M. G.; Johnson, A. L.; Leong, B. K. L.; McIndoe, J. S.; Pomeroy, R. K.; Raithby, P. R.; Sappa, E.; Suzuki, H.; Takao, T.; Thomas, D.; Whittlesey, M. K.; Wilton-Ely, J. D.; Wong, W.-T. In *Comprehensive Organometallic Chemistry III*; Crabtree, R. H., Mingos, D. M. P., Eds.; Pergamon Press: Oxford, U.K., 2007; Vol. *6*, pp 353−1116.

(2) Selected recent reviews: (a) Samojłowicz, C.; Bieniek, M.; Grela, K. *Chem. Rev.* **2009**, *109*, 3708. (b) Concepcion, J. J.; Jurss, J. W.; Brennaman, M. K.; Hoertz, P. G.; Patrocinio, A. O. T.; Murakami Iha, N. Y.; Templeton, J. L.; Meyer, T. J. *Acc. Chem. Res.* **2009**, *42*, 1954. (c) Nolan, S. P.; Clavier, H. *Chem. Soc. Rev.* **2010**, *39*, 3305. (d) Muratsugu, S.; Tada, M. *Acc. Chem. Res.* **2013**, *46*, 300. (e) Kozhushkov, S. I.; Ackermann, L. *Chem. Sci.* **2013**, *4*, 886.

(3) Selected recent reviews: (a) Ang, W. H.; Dyson, P. J. *Eur. J. Inorg. Chem.* **2006**, 4003. (b) Bruijnincx, P. C. A.; Sadler, P. J. *Adv. Inorg. Chem.* **2009**, *61*, 1. (c) Süss-Fink, G. *Dalton Trans.* **2010**, *39*, 1673. (d) Smith, G. S.; Therrien, B. *Dalton Trans.* **2011**, *40*, 10793. (e) Noffke, A. L.; Habtemariam, A.; Pizarro, A. M.; Sadler, P. J. *Chem. Commun.* **2012**, *48*, 5219.

(4) Selected recent reviews: (a) Balzani, V.; Juris, A. *Coord. Chem. Rev.* **2001**, *211*, 97. (b) Vos, J. G.; Kelly, J. M. *Dalton Trans.* **2006**, 4869. (c) Campagna, S.; Puntoriero, F.; Nastasi, F.; Bergamini, G.; Balzani, V. *Top. Curr. Chem.* **2007**, *280*, 117. (d) Herman, L.; Ghosh, S.; Defrancq, E.; Kirsch-De Mesmaeker, A. *J. Phys. Org. Chem.* **2008**, *21*, 670. (e) Bonnet, S.; Collin, J.-P. *Chem. Soc. Rev.* **2008**, *37*, 1207.

(5) Selected examples: (a) Buda, M.; Kalyuzhny, G.; Bard, A. J. *J. Am. Chem. Soc.* **2002**, *124*, 6090. (b) Welter, S.; Brunner, K.; Hofstraat, J. W.; De Cola, L. *Nature* **2003**, *421*, 54. (c) Tung, Y.-L.; Chen, L.-S.; Chi, Y.; Chou, P.-T.; Cheng, Y.-M.; Li, E. Y.; Lee, G.-H.; Shu, C.-F.; Wu, F.-I.; Carty, A. J. *Adv. Funct. Mater.* **2006**, *16*, 1615. (d) Chou, P.-T.; Chi, Y. *Chem.—Eur. J.* **2007**, *13*, 380. (e) Zhu, Y.-Y.; Gu, C.; Tang, S.; Fei, T.; Gu, X.; Wang, H.; Wang, Z.-M.; Wang, F.-F.; Lu, D.; Ma, Y.-G. *J. Mater. Chem.* **2009**, *19*, 3941.

(6) Selected recent reviews: (a) Ardo, S.; Meyer, G. J. *Chem. Soc. Rev.* **2009**, *38*, 115. (b) Hagfeldt, A.; Boschloo, G.; Sun, L.-C.; Kloo, L.; Pettersson, H. *Chem. Rev.* **2010**, *110*, 6595. (c) Clifford, J. N.; Martínez-Ferrero, E.; Viterisi, A.; Palomares, E. *Chem. Soc. Rev.* **2011**, *40*, 1635. (d) Reynal, A.; Palomares, E. *Eur. J. Inorg. Chem.* **2011**, 4509. (e) Robson, K. C. D.; Bomben, P. G.; Berlinguette, C. P. *Dalton Trans.* **2012**, *41*, 7814.

(7) Recent reviews on NLO-active metal complexes, with a substantial coverage of Ru: (a) Coe, B. J. In *Comprehensive Coordination Chemistry II*; McCleverty, J. A., Meyer, T. J., Eds.; Elsevier Pergamon: Oxford, U.K., 2004; Vol. *9*, pp 621−687. (b) Maury, O.; Le Bozec, H. *Acc. Chem. Res.* **2005**, *38*, 691. (c) Coe, B. J. *Acc. Chem. Res.* **2006**, *39*, 383. (d) Coe, B. J. In *Nonlinear Optical Properties of Matter: From Molecules to Condensed Phases*; Papadopoulos, M. G., Leszczynski, J., Sadlej, A. J., Eds.; Springer: Dordrecht, 2006; pp 571−608. (e) Morrall, J. P.; Dalton, G. T.; Humphrey, M. G.; Samoc, M. *Adv. Organomet. Chem.* **2007**, *55*, 61. (f) Di Bella, S.; Dragonetti, C.; Pizzotti, M.; Roberto, D.; Tessore, F.; Ugo, R. *Top. Organomet. Chem.* **2010**, *28*, 1. (g) Maury, O.; Le Bozec, H. In *Molecular Materials*; Bruce, D. W., O'Hare, D., Walton,

R. I., Eds.; Wiley: Chichester, U.K., 2010; pp 1−59. (h) Coe, B. J. *Coord. Chem. Rev.* **2013**, *257*, 1438.
(8) (a) *Nonlinear Optics of Organic Molecules and Polymers*; Nalwa, H. S., Miyata, S., Eds.; CRC Press: Boca Raton, FL, 1997. (b) *Nonlinear Optical Properties of Matter: From Molecules to Condensed Phases*; Papadopoulos, M. G., Leszczynski, J., Sadlej, A. J., Eds.; Springer: Dordrecht, 2006. (c) De Meulenaere, E.; Chen, W.-Q.; Van Cleuvenbergen, S.; Zheng, M.-L.; Psilodimitrakopoulos, S.; Paesen, R.; Taymans, J.-M.; Ameloot, M.; Vanderleyden, J.; Loza-Alvarez, P.; Duan, X.-M.; Clays, K. *Chem. Sci.* **2012**, *3*, 984 and references therein.
(9) (a) Coe, B. J.; Harris, J. A.; Jones, L. A.; Brunschwig, B. S.; Song, K.; Clays, K.; Garín, J.; Orduna, J.; Coles, S. J.; Hursthouse, M. B. *J. Am. Chem. Soc.* **2005**, *127*, 4845. (b) Coe, B. J.; Foxon, S. P.; Harper, E. C.; Helliwell, M.; Raftery, J.; Swanson, C. A.; Brunschwig, B. S.; Clays, K.; Franz, E.; Garín, J.; Orduna, J.; Horton, P. N.; Hursthouse, M. B. *J. Am. Chem. Soc.* **2010**, *132*, 1706.
(10) Selected examples: (a) Barqawi, K. R.; Llobet, A.; Meyer, T. J. *J. Am. Chem. Soc.* **1988**, *110*, 7751. (b) Llobet, A.; Curry, M. E.; Evans, H. T.; Meyer, T. J. *Inorg. Chem.* **1989**, *28*, 3131. (c) Jones, W. E., Jr.; Bignozzi, C. A.; Chen, P.-Y.; Meyer, T. J. *Inorg. Chem.* **1993**, *32*, 1167. (d) Field, L. D.; Messerle, B. A.; Soler, L.; Buys, I. E.; Hambley, T. W. *J. Chem. Soc., Dalton Trans.* **2001**, 1959. (e) Wilson, D. C.; Nelson, J. H. *J. Organomet. Chem.* **2003**, *682*, 272. (f) Katz, N. E.; Romero, I.; Llobet, A.; Parella, T.; Benet-Buchholz, J. *Eur. J. Inorg. Chem.* **2005**, 272. (g) Iengo, E.; Zangrando, E.; Baiutti, E.; Munini, F.; Alessio, E. *Eur. J. Inorg. Chem.* **2005**, 1019. (h) Katz, N. E.; Fagalde, F.; Lis de Katz, N. D.; Mellace, M. G.; Romero, I.; Llobet, A.; Benet-Buchholz, J. *Eur. J. Inorg. Chem.* **2005**, 3019. (i) Foxon, S. P.; Metcalfe, C.; Adams, H.; Webb, M.; Thomas, J. A. *Inorg. Chem.* **2007**, *46*, 409. (j) Kuzu, I.; Nied, D.; Breher, F. *Eur. J. Inorg. Chem.* **2009**, 872. (k) Waywell, P.; Gonzalez, V.; Gill, M. R.; Adams, H.; Meijer, A. J. H. M.; Williamson, M. P.; Thomas, J. A. *Chem.—Eur. J.* **2010**, *16*, 2407. (l) De, P.; Mondal, T. K.; Mobin, S. M.; Lahiri, G. K. *Inorg. Chim. Acta* **2011**, *372*, 250. (m) Agarwala, H.; Das, D.; Mobin, S. M.; Mondal, T. K.; Lahiri, G. K. *Inorg. Chim. Acta* **2011**, *374*, 216. (n) Serrano, I.; López, M. I.; Ferrer, I.; Poater, A.; Parella, T.; Fontrodona, X.; Solà, M.; Llobet, A.; Rodríguez, M.; Romero, I. *Inorg. Chem.* **2011**, *50*, 6044. (o) Zagermann, J.; Klein, K.; Merz, K.; Molon, M.; Metzler-Nolte, N. *Eur. J. Inorg. Chem.* **2011**, 4212. (p) Cadranel, A.; Alborés, P.; Yamazaki, S.; Kleiman, V. D.; Baraldo, L. M. *Dalton Trans.* **2012**, *41*, 5343. (q) Agarwala, H.; Ehret, F.; Chowdhury, A. D.; Maji, S.; Mobin, S. M.; Kaim, W.; Lahiri, G. K. *Dalton Trans.* **2013**, *42*, 3721. (r) Guelfi, M.; Puntoriero, F.; Arrigo, A.; Serroni, S.; Cifelli, M.; Denti, G. *Inorg. Chim. Acta* **2013**, *398*, 19. (s) Coe, B. J.; Raftery, J.; Rusanova, D. *Acta Crystallogr., Sect. E* **2013**, *69*, m549.
(11) Reger, D. L.; Grattan, T. C.; Brown, K. J.; Little, C. A.; Lamba, J. J. S.; Rheingold, A. L.; Sommer, R. D. *J. Organomet. Chem.* **2000**, *607*, 120.
(12) Llobet, A.; Doppelt, P.; Meyer, T. J. *Inorg. Chem.* **1988**, *27*, 514.
(13) Xu, H.-J.; Cheng, Y.; Sun, J.-F.; Dougan, B. A.; Li, Y.-Z.; Chen, X.-T.; Xue, Z.-L. *J. Organomet. Chem.* **2008**, *693*, 3851.
(14) Yonemoto, E. H.; Riley, R. L.; Kim, Y. I.; Atherton, S. J.; Schmehl, R. H.; Mallouk, T. E. *J. Am. Chem. Soc.* **1992**, *114*, 8081.
(15) Coe, B. J.; Harris, J. A.; Harrington, L. J.; Jeffery, J. C.; Rees, L. H.; Houbrechts, S.; Persoons, A. *Inorg. Chem.* **1998**, *37*, 3391.
(16) *SAINT* (Version 6.45) and *SADABS* (Version 2.10); Bruker AXS Inc.: Madison, Wisconsin, USA, 2003.
(17) Sheldrick, G. M. *Acta Crystallogr., Sect. A* **1990**, *46*, 467.
(18) Sheldrick, G. M. *SHELXL 97*, Program for crystal structure refinement; University of Göttingen: Göttingen, Germany, 1997.
(19) *SHELXTL* (Version 6.10); Bruker AXS Inc.: Madison, Wisconsin, USA, 2000.
(20) (a) Olbrechts, G.; Strobbe, R.; Clays, K.; Persoons, A. *Rev. Sci. Instrum.* **1998**, *69*, 2233. (b) Olbrechts, G.; Wostyn, K.; Clays, K.; Persoons, A. *Opt. Lett.* **1999**, *24*, 403. (c) Clays, K.; Wostyn, K.; Olbrechts, G.; Persoons, A.; Watanabe, A.; Nogi, K.; Duan, X.-M.; Okada, S.; Oikawa, H.; Nakanishi, H.; Vogel, H.; Beljonne, D.; Brédas, J.-L. *J. Opt. Soc. Am. B* **2000**, *17*, 256.
(21) Heesink, G. J. T.; Ruiter, A. G. T.; van Hulst, N. F.; Bölger, B. *Phys. Rev. Lett.* **1993**, *71*, 999.
(22) (a) Shin, Y. K.; Brunschwig, B. S.; Creutz, C.; Sutin, N. *J. Phys. Chem.* **1996**, *100*, 8157. (b) Coe, B. J.; Harris, J. A.; Brunschwig, B. S. *J. Phys. Chem. A* **2002**, *106*, 897.
(23) (a) Liptay, W. In *Excited States*; Lim, E. C., Ed.; Academic Press: New York, 1974; Vol. *1*, pp 129−229. (b) Bublitz, G. U.; Boxer, S. G. *Annu. Rev. Phys. Chem.* **1997**, *48*, 213. (c) Brunschwig, B. S.; Creutz, C.; Sutin, N. *Coord. Chem. Rev.* **1998**, *177*, 61.
(24) Frisch, M. J.; Trucks, G. W.; Schlegel, H. B.; Scuseria, G. E.; Robb, M. A.; Cheeseman, J. R.; Scalmani, G.; Barone, V.; Mennucci, B.; Petersson, G. A.; Nakatsuji, H.; Caricato, M.; Li, X.; Hratchian, H. P.; Izmaylov, A. F.; Bloino, J.; Zheng, G.; Sonnenberg, J. L.; Hada, M.; Ehara, M.; Toyota, K.; Fukuda, R.; Hasegawa, J.; Ishida, M.; Nakajima, T.; Honda, Y.; Kitao, O.; Nakai, H.; Vreven, T.; Montgomery, J. A., Jr.; Peralta, J. E.; Ogliaro, F.; Bearpark, M.; Heyd, J. J.; Brothers, E.; Kudin, K. N.; Staroverov, V. N.; Kobayashi, R.; Normand, J.; Raghavachari, K.; Rendell, A.; Burant, J. C.; Iyengar, S. S.; Tomasi, J.; Cossi, M.; Rega, N.; Millam, N. J.; Klene, M.; Knox, J. E.; Cross, J. B.; Bakken, V.; Adamo, C.; Jaramillo, J.; Gomperts, R.; Stratmann, R. E.; Yazyev, O.; Austin, A. J.; Cammi, R.; Pomelli, C.; Ochterski, J. W.; Martin, R. L.; Morokuma, K.; Zakrzewski, V. G.; Voth, G. A.; Salvador, P.; Dannenberg, J. J.; Dapprich, S.; Daniels, A. D.; Farkas, Ö.; Foresman, J. B.; Ortiz, J. V.; Cioslowski, J.; Fox, D. J. *Gaussian 09, Revision A.02*; Gaussian, Inc.: Wallingford, CT, 2009.
(25) (a) Perdew, J. P. *Phys. Rev. B* **1986**, *33*, 8822. (b) Becke, A. D. *Phys. Rev. A* **1988**, *38*, 3098.
(26) Becke, A. D. *J. Chem. Phys.* **1993**, *98*, 5648.
(27) Yanai, T.; Tew, D. P.; Handy, N. C. *Chem. Phys. Lett.* **2004**, *393*, 51.
(28) Adamo, C.; Barone, V. *J. Chem. Phys.* **1999**, *110*, 6158.
(29) Zhao, Y.; Truhlar, D. *Theor. Chem. Acc.* **2008**, *120*, 215.
(30) (a) Hay, P. J.; Wadt, W. R. *J. Chem. Phys.* **1985**, *82*, 270. (b) Hay, P. J.; Wadt, W. R. *J. Chem. Phys.* **1985**, *82*, 299.
(31) (a) Barone, V.; Cossi, M. *J. Phys. Chem. A* **1998**, *102*, 1995. (b) Cossi, M.; Rega, N.; Scalmani, G.; Barone, V. *J. Comput. Chem.* **2003**, *24*, 669.
(32) O'Boyle, N. M.; Tenderholt, A. L.; Langner, K. M. *J. Comput. Chem.* **2008**, *29*, 839.
(33) Thanthiriwatte, K. S.; Nalin de Silva, K. M. *J. Mol. Struct.: THEOCHEM* **2002**, *617*, 169.
(34) Selected examples: (a) Adeyemi, S. A.; Miller, F. J.; Meyer, T. J. *Inorg. Chem.* **1972**, *11*, 994. (b) Adeyemi, S. A.; Johnson, E. C.; Miller, F. J.; Meyer, T. J. *Inorg. Chem.* **1973**, *12*, 2371. (c) Coe, B. J.; Meyer, T. J.; White, P. S. *Inorg. Chem.* **1995**, *34*, 593. (d) Coe, B. J.; Chery, M.; Beddoes, R. L.; Hope, H.; White, P. S. *J. Chem. Soc., Dalton Trans.* **1996**, 3917. (e) Coe, B. J.; Beyer, T.; Jeffery, J. C.; Coles, S. J.; Gelbrich, T.; Hursthouse, M. B.; Light, M. E. *J. Chem. Soc., Dalton Trans.* **2000**, 797.
(35) (a) Coe, B. J. *Chem.—Eur. J.* **1999**, *5*, 2464. (b) Asselberghs, I.; Clays, K.; Persoons, A.; Ward, M. D.; McCleverty, J. A. *J. Mater. Chem.* **2004**, *14*, 2831.
(36) Coe, B. J.; Jones, L. A.; Harris, J. A.; Sanderson, E. E.; Brunschwig, B. S.; Asselberghs, I.; Clays, K.; Persoons, A. *Dalton Trans.* **2003**, 2335.
(37) Laurent, F.; Plantalech, E.; Donnadieu, B.; Jiménez, A.; Hernández, F.; Martínez-Ripoll, M.; Biner, M.; Llobet, A. *Polyhedron* **1999**, *18*, 3321.
(38) Maurer, J.; Linseis, M.; Sarkar, B.; Schwederski, B.; Niemeyer, M.; Kaim, W.; Záliš, S.; Anson, C.; Zabel, M.; Winter, R. F. *J. Am. Chem. Soc.* **2008**, *130*, 259.
(39) Coe, B. J.; Harris, J. A.; Asselberghs, I.; Persoons, A.; Jeffery, J. C.; Rees, L. H.; Gelbrich, T.; Hursthouse, M. B. *J. Chem. Soc., Dalton Trans.* **1999**, 3617.
(40) (a) Oudar, J. L.; Chemla, D. S. *J. Chem. Phys.* **1977**, *66*, 2664. (b) Oudar, J. L. *J. Chem. Phys.* **1977**, *67*, 446.

(41) Coe, B. J.; Foxon, S. P.; Harper, E. C.; Harris, J. A.; Helliwell, M.; Raftery, J.; Asselberghs, I.; Clays, K.; Franz, E.; Brunschwig, B. S.; Fitch, A. G. *Dyes Pigm.* **2009**, *82*, 171.
(42) Coe, B. J.; Harris, J. A.; Asselberghs, I.; Wostyn, K.; Clays, K.; Persoons, A.; Brunschwig, B. S.; Coles, S. J.; Gelbrich, T.; Light, M. E.; Hursthouse, M. B.; Nakatani, K. *Adv. Funct. Mater.* **2003**, *13*, 347.
(43) Coe, B. J.; Pilkington, R. A. *J. Phys. Chem.* **2014**, *118* in press , DOI: 10.1021/jp4114927.